ISSN 0016-7037
Volume 72, Number 23
December 1, 2008

ELSEVIER

Geochimica et Cosmochimica Acta

JOURNAL OF THE GEOCHEMICAL SOCIETY
AND THE METEORITICAL SOCIETY

Volume 72, Number 23 December 1, 2008

Articles

Continued on outside back cover

Available online at www.sciencedirect.com
ScienceDirect
Geochimica et Cosmochimica Acta 72 (2008) 5641–5658
Geochimica et Cosmochimica Acta
www.elsevier.com/locate/gca

Characterization of calcium isotopes in natural and synthetic barite

Elizabeth M. Griffith [a,b,*], Edwin A. Schauble [c], Thomas D. Bullen [d], Adina Paytan [b]

[a] Department of Geological & Environmental Sciences, Stanford University, Building 320, Room 118, Stanford, CA 94305, USA
[b] Institute of Marine Sciences, University of California, Santa Cruz, CA 95064, USA
[c] Department of Earth and Space Sciences, University of California, Los Angeles, 595 Charles Young Drive East, Box 951567, Los Angeles, CA 90095, USA
[d] Branch of Regional Research, Water Resources Division, U.S. Geological Survey, MS 420, 345 Middlefield Rd., Menlo Park, CA 94025, USA

Received 25 February 2008; accepted in revised form 18 August 2008; available online 26 August 2008

Abstract

The mineral barite ($BaSO_4$) accommodates calcium in its crystal lattice, providing an archive of Ca-isotopes in the highly stable sulfate mineral. Holocene marine (pelagic) barite samples from the major ocean basins are isotopically indistinguishable from each other ($\delta^{44/40}Ca = -2.01 \pm 0.15‰$) but are different from hydrothermal and cold seep barite samples ($\delta^{44/40}Ca = -4.13$ to $-2.72‰$). Laboratory precipitated (synthetic) barite samples are more depleted in the heavy Ca-isotopes than pelagic marine barite and span a range of Ca-isotope compositions, $\Delta^{44/40}Ca = -3.42$ to $-2.40‰$. Temperature, saturation state, $a{Ba^{2+}}/a{SO_4^{2-}}$, and $a{Ca^{2+}}/a{Ba^{2+}}$ each influence the fractionation of Ca-isotopes in synthetic barite; however, the fractionation in marine barite samples is not strongly related to any measured environmental parameter. First-principles lattice dynamical modeling predicts that at equilibrium Ca-substituted barite will have much lower $^{44}Ca/^{40}Ca$ than calcite, by $-9‰$ at 0 °C and $-8‰$ at 25 °C. Based on this model, none of the measured barite samples appear to be in isotopic equilibrium with their parent solutions, although as predicted they do record lower $\delta^{44/40}Ca$ values than seawater and calcite. Kinetic fractionation processes therefore most likely control the extent of isotopic fractionation exhibited in barite. Potential fractionation mechanisms include factors influencing Ca^{2+} substitution for Ba^{2+} in barite (e.g. ionic strength and trace element concentration of the solution, competing complexation reactions, precipitation or growth rate, temperature, pressure, and saturation state) as well as nucleation and crystal growth rates. These factors should be considered when investigating controls on isotopic fractionation of Ca^{2+} and other elements in inorganic and biogenic minerals.

1. INTRODUCTION

In this study we investigated fractionation processes affecting calcium (Ca) isotopes during barite precipitation, in order to validate the use of Ca-isotopes in marine (pelagic) barite as a recorder of solution (seawater) chemistry, and to highlight potential fractionation mechanisms during trace element incorporation. This was done by (1) estimating the expected equilibrium fractionation of Ca in barite using first-principles lattice dynamical models of a Ca-substituted barite structure, (2) analyzing naturally occurring marine barite and other types of natural barite (hydrothermal and cold seep) from a wide range of locations, and (3) precipitating barite in the laboratory under various conditions that might influence Ca-isotope fractionation.

Ca-isotopes are valuable in determining changes in the global biogeochemical cycling of Ca and carbon (C) on various time scales (Zhu and Macdougall, 1998; De La Rocha and DePaolo, 2000; Schmitt et al., 2003b; Soudry et al., 2004; Fantle and DePaolo, 2005; Heuser et al., 2005; Kasemann et al., 2005; Steuber and Buhl, 2006;

* Corresponding author.
E-mail address: emgriffith@stanford.edu (E.M. Griffith).

0016-7037/$ - see front matter © 2008 Elsevier Ltd. All rights reserved.
doi:10.1016/j.gca.2008.08.010

Farkaš et al., 2007; Sime et al., 2007). Although the specific parameters controlling Ca-isotope systematics in different settings are not well understood (e.g. Fantle and DePaolo, 2007; Sime et al., 2007), it is generally thought that both kinetic and equilibrium isotope fractionation processes are involved.

Differences in Ca-isotope ratios between minerals are typically thought to be controlled by equilibrium isotope fractionation mechanics (Gussone et al., 2005), although kinetic effects at the crystal surface might also explain these differences. The degree of equilibrium isotopic fractionation of Ca between minerals is likely to reflect the coordination number of Ca within these minerals, similar to other main group lithophile metals like Li, Mg, and Si (Schauble, 2004).

Kinetic isotope fractionations, those resulting from unidirectional processes under conditions of incomplete isotopic exchange, can be sensitive to a host of factors (e.g. reaction rates, presence of exchange catalysts, temperature). It is often difficult to distinguish between the relative contributions of equilibrium versus kinetic effects, although for inorganic calcite precipitated in the laboratory, Lemarchand et al. (2004) demonstrated that kinetic isotope effects were indeed present.

Precise equilibrium isotopic fractionation between minerals is difficult to determine either empirically or theoretically. It is usually impossible to directly calculate the equilibrium isotope fractionation for a particular mineral pair due to the lack of measurements of vibrational spectra for uncommon isotopic forms. Instead it may be necessary to rely on complex empirical force-field calculations or *ab initio* quantum chemistry (Schauble, 2004) to determine if equilibrium isotope fractionation controls differences in Ca-isotope ratios between measured samples.

Most geologic studies have focused on measuring Ca-isotopes in minerals that have Ca as a major component such as calcite, aragonite, or apatite. However, Ca can also be incorporated in trace amounts within other minerals, substituting for the major cation(s). For example, the mineral barite ($BaSO_4$) can support up to 6% substitution of Ca^{2+} for Ba^{2+} in its crystal lattice (Hennessy and Graham, 2002), although natural barite samples typically contain much lower Ca concentrations (~400 ppm; Averyt and Paytan, 2003). Trace element incorporation into a solid is influenced by many parameters, including the ionic strength and trace element concentration of the solution, competing complexation reactions, precipitation or growth rate, temperature, pressure, and saturation state (e.g. Jones et al., 2004). These parameters are likely to affect equilibrium and/or kinetic isotopic fractionation of the trace element in the precipitated mineral.

Barite forms inorganically in the ocean when relatively Ba^{2+}-rich fluids mix with SO_4^{2-}-rich fluids. This may occur within sediments (diagenetic barite) and at or near the seafloor, either in association with hydrothermal activity (hydrothermal barite) or in the absence of hydrothermal activity (cold seep barite) (e.g. Paytan et al., 2002). Barite also precipitates within the water column (marine or pelagic barite) in microenvironments containing decaying Ba-rich organic matter and other biogenic debris (e.g. Chow and Goldberg, 1960; Dehairs et al., 1980; Bishop, 1988; Stroobants et al., 1991; Ganeshram et al., 2003).

2. NOTATION AND METHODS

2.1. Notation

The Ca-isotope composition of a sample is expressed as the deviation from a standard solution value, using δ-notation in permil:

$$\delta^{44/40}\mathrm{Ca} = [(^{44}\mathrm{Ca}/^{40}\mathrm{Ca}_{\mathrm{sample}} - {}^{44}\mathrm{Ca}/^{40}\mathrm{Ca}_{\mathrm{standard}})/{}^{44}\mathrm{Ca}/^{40}\mathrm{Ca}_{\mathrm{standard}}] \times 1000 \quad (1)$$

where $^{44}Ca/^{40}Ca_{standard}$ refers to the $^{44}Ca/^{40}Ca$ isotope ratio of seawater.

In order to compare isotopic fractionation between a precipitated solid ($\delta^{44/40}Ca_{solid}$) and its original parent solution ($\delta^{44/40}Ca_{solution}$), the follow representation is used in permil:

$$\Delta^{44/40}\mathrm{Ca} = \delta^{44/40}\mathrm{Ca}_{\mathrm{solid}} - \delta^{44/40}\mathrm{Ca}_{\mathrm{solution}} \quad (2)$$

2.2. Modeling methods

A rough theoretical estimate of the likely equilibrium Ca-isotope fractionation between Ca-substituted barite and dissolved Ca in seawater was obtained by first-principles lattice dynamics modeling. Models of barite, Ca-substituted barite, and calcite were constructed using the plane-wave density functional theory code PWscf (Baroni et al., www.pwscf.org). Ca-isotope fractionation factors for calcite and Ca-substituted barite were calculated following the procedure of Schauble et al. (2006), by sampling phonon frequencies of ^{40}Ca and ^{44}Ca-substituted crystals at non-zero phonon wave vectors (one wave vector for barite, two for calcite) and using the frequencies to estimate reduced partition function ratios for Ca-isotope exchange (e.g. Urey, 1947).

Pure barite was modeled as a starting point for examining Ca-substitution, and provided a point of comparison with experimental structures and phonon frequencies. Ca-substituted barite was modeled in both a regular barite unit cell and a $1 \times 1 \times 2$ supercell (i.e. doubled along the shortest crystal axis). In each model, one Ca atom was swapped into a Ba site in the crystal. These models correspond to perfectly ordered 25% mol. and 12.5% mol. $CaSO_4$ substitutions. Although representing higher Ca:Ba ratios than found in natural barites, empirical potential studies suggest that these models will provide a reasonably accurate first-order representation of trace substitution.

To investigate the potential effects of Ca concentration on Ca-isotope equilibrium fractionation in barite, we examined a number of hypothetical structures of Ca-substituted barite, using the empirical potentials of Wahid et al. (2002). These empirical potential models can be extended to much larger supercells than are tractable with the more computationally intensive density functional theory (DFT). Minimum-energy Ca–O bond lengths in these supercell structures (Table 1) suggest that the inner coordination

Table 1
Comparison of supercell structures from density function theory (DFT) and empirical potential models

	DFT models		Empirical potential models			
Supercell dimensions	1 × 1 × 1	1 × 1 × 2	1 × 1 × 1	1 × 1 × 2	2 × 2 × 2	3 × 3 × 3
mol % $CaSO_4$	25.0%	12.5%	25.0%	12.5%	3.1%	0.9%
Mean *r*(Ca–O) of:						
6 shortest Ca–O bonds	2.563	2.53	2.608	2.566	2.6	2.597
8 shortest Ca–O bonds	2.603	2.665	2.714	2.689	2.683	2.682
10 shortest Ca–O bonds	2.736	2.76	2.785	2.783	2.788	2.789
12 shortest Ca–O bonds	2.885	2.88	2.888	2.899	2.9	2.901

polyhedra around Ca^{2+} in 25% and 12.5% mol. substituted barites are very similar to those coordinating Ca^{2+} defects in 2 × 2 × 2 or 3 × 3 × 3 supercells (3.125% and 0.926% mol. $CaSO_4$, respectively). Equilibrium isotopic fractionation is largely determined by the force constants of the stiffest (i.e. shortest) bonds acting on the atom of interest (Bigeleisen and Mayer, 1947), so the similarity in average Ca–O bond lengths over a range of Ca concentrations indicates that equilibrium Ca-isotope fractionations calculated for hypothetical Ca-rich (DFT model) barites are likely to be close to equilibrium fractionations in Ca-poor (natural or synthetic) barite.

In constructing the first-principles models of Ca-substituted barite, an initial relaxation was performed with the substituted calcium atom positioned at the same crystal site as barium. Before final relaxation, the substituted calcium atom was shifted slightly ($\ll$0.1 Å) in a random direction, to remove all mirror-plane and rotational symmetry in the substituted structure. The inversion symmetry of pure barite was destroyed by the initial Ca:Ba substitution, and this, along with the random positional shift, prevented the substituted structure from relaxing to an unstable state with false symmetry. The unit cell shape and perturbed atomic positions were then fully relaxed as described below.

The calcite model was generated as a point of comparison between barite and seawater, since experimental studies suggest that the equilibrium Ca-isotope fractionation between calcite and water is relatively small ($\sim$1.5‰ Lemarchand et al., 2004; $\sim$0‰ Fantle and DePaolo, 2007), and the structure and vibrational frequency spectrum of calcite are relatively simple and well-studied. It is hoped that potential systematic errors in the present first-principles models of Ca-substituted barite will be partially cancelled by direct comparison to a similarly constructed calcite model.

Previous work has shown that quantum mechanical models, calculated with density functional theory, provide reasonably accurate estimates of known oxygen and carbon isotope fractionations in carbonate and silicate minerals (Schauble et al., 2006; Méheut et al., 2007). Models of calcite and barite in the present study follow this basic methodology. Density functional theory, in principle mathematically equivalent to Schrodinger's equation, is only tractable in complex materials if simplifying assumptions are followed. In the present work, all calculations use a gradient-corrected density functional (PBE; Perdew et al., 1996), and publicly available ultrasoft pseudopotentials for calcium, barium, sulfur, carbon and oxygen (www.pwscf.org). The PBE functional provides a computationally efficient description of electron exchange and correlation effects, while the pseudopotentials simplify calculations by replacing non-valence electrons with an effective core potential. For some elements it is helpful to treat the outermost non-valence electrons as if they were chemically active (semi-core), even though this slightly increases the computational expense. The calcium pseudopotential included semi-core 3s and 3p electrons in valence (i.e. a reference configuration of $[Ne]3s^23p^64s^23d^0$). The barium pseudopotential included 5s and 5p electrons in valence (reference configuration $[Kr+4d^{10}]5s^25p^65d^06s^26p^0$), as well as a nonlinear core correction for non-valence electrons. All of the pseudopotentials except carbon were generated with scalar-relativistic calculations.

In addition to these simplifications, there are additional parameters that affect the precision of each model. These include the number of plane waves in the basis set (expressed as a maximum or cutoff energy) and the number of electronic wave vectors used to construct the electronic structure. In DFT studies, these two parameters are usually varied by progressively increasing the cutoff energy and sample of wave vectors (and thus the accuracy of the model) until the calculated energy of the model structure converges. In this study, the cell parameters (especially the unit cell size) rather than the structural energy were used to test convergence, because the former converge more slowly as the cutoff energy is increased.

Ultrasoft pseudopotentials, the type used in this study, are particularly useful for studying large, low symmetry structures like Ca-substituted barite because they generally converge at lower cutoff energies than other pseudopotential types. A cutoff energy of 40 Rydberg (544 eV) for the plane-wave basis sets seems to be sufficient to achieve $\sim$0.1% convergence in unit cell parameters for all model structures. This cutoff is used in all structural relaxations and vibrational (phonon) frequency calculations.

The barite and Ca-substituted barite models were calculated using an offset 2 × 2 × 2 wave-vector grid (Monkhorst and Pack, 1976), with four distinct electronic wave vectors, while the calcite model used a six-vector, 3 × 3 × 3 grid. A finer grid for calcite is needed because the unit cell is much smaller than barite. In each case, the chosen wave-vector grid yields unit-cell parameters within $\sim$0.1% of finer grids. The accuracies of the first-principles models were checked by comparing model unit cell parameters and Raman or IR-active phonon frequencies with experiments.

Models of each crystal were optimized, allowing relaxation of atomic positions and unit cell parameters, until the residual forces on each atom were less than 10^{-4} Rydberg/

Bohr ($\sim 4 \times 10^{-12}$ N) and every component of stress acting on unit cells was less than 0.5 kbar.

2.3. Analytical methods

2.3.1. Natural samples

Holocene marine (pelagic) barite was separated from deep-sea coretop sediments representing most major ocean basins (Fig. 1) using a sequential acid leaching procedure (Paytan et al., 1993; Martin et al., 1995; Eagle et al., 2003). Marine barite is morphologically distinct from hydrothermal, cold seep, and diagenetic barite crystals, having characteristically small (few μm sized) euhedral, elliptical or spherical crystals (Fig. 2). The recovery yield of this separation method is high (~95%; Eagle et al., 2003) and no reprecipitation of barite or isotopic redistribution of Sr occurs (Paytan et al., 1993) which is assumed to hold true for Ca. Purity of the insoluble residue of the sequential leaching procedure and morphology of the barite crystals was checked using scanning electron microscopy with energy dispersive X-ray spectroscopy (SEM-EDS). If the samples were not pure (<95% barite), leaching steps were repeated until the desired purity (>95% barite) was established. Ti oxides and some highly refractory non-barite minerals often remain after the described leaching process and these must constitute less than 5% of the residue for reliable Ca-isotope analysis. Analyses of samples with >5% non-barite minerals in the sample residue resulted in much higher $\delta^{44/40}$Ca values than pure coretop marine barite samples, being closer to bulk Earth estimates (−0.84‰; Fantle and DePaolo, 2005). Intense screening of each sample is imperative because of the low concentrations of Ca in marine barite (~400 ppm) and the possibility for non-barite Ca inclusion from the refractory minerals in the sample residue.

Hydrothermal and cold seep pure (>95%) barite samples with characteristic cross-cutting tabular crystals and rosettes (sand rose structures) larger than 20 μm were also analyzed (Figs. 1 and 2). Hydrothermal barite samples come from chimneys on the Juan de Fuca Ridge (JdFR) (Reyes et al., 1995) and the Mid-Atlantic Ridge (Tivey et al., 1995) and massive barite from the Guaymas Basin (Lonsdale and Becker, 1985). Cold seep barite samples were taken from the San Clemente fault zone off San Diego, California (Lonsdale, 1979; Torres et al., 2002) and dredged samples collected near Ensenada, Baja California (Legg, 1980). Purity was confirmed using SEM-EDS. Prior to dissolution, samples were rinsed with 8 M nitric acid and ultra-pure Milli-Q water to dissolve any potential surface contaminants.

2.3.2. Laboratory precipitation experiments

Experiments were designed to test the influence of changing temperature, initial saturation state, and solution chemistry (e.g. $a\mathrm{Ba}^{2+}/a\mathrm{SO_4}^{2-}$, Ca concentration) on the isotopic fractionation of Ca in barite. All experiments were preformed with $[\mathrm{SO_4}^{2-}]$ in excess with respect to $[\mathrm{Ba}^{2+}]$ because this is most similar to natural conditions in the modern ocean. However, the saturation indexes of all of the experiments (S.I. = 2.3–3.97) were much higher than those in the oceanic water column (Monnin and Cividini, 2006) in order to precipitate ample barite from manageable volumes of solution in the laboratory.

Seawater from the Pacific Ocean collected close to Santa Cruz, California was filtered with 0.22 μm pore-sized membrane filters (Millipore type GSWP) and used as a medium for barite precipitation (pH 8.2). $BaCl_2$ (barium chloride dihydrate, Fisher Chemical B34-500), $CaCl_2$ (calcium chloride dihydrate, Sigma C2536), and Na_2SO_4 (sodium sulfate, anhydrous, Fisher Chemical S93381) were dissolved in ultra-pure Milli-Q water to produce precipitation/feed

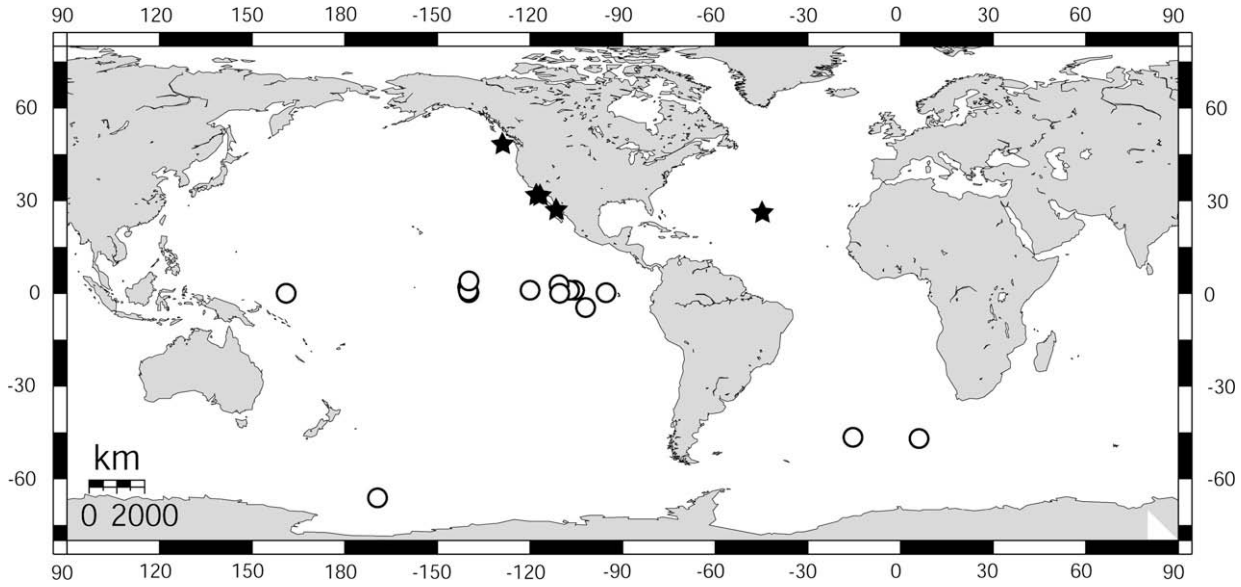

Fig. 1. Locations of natural barite samples. Open circles are Holocene marine (pelagic) barite samples. Filled stars are hydrothermal and cold seep barite samples. Map was created using Online Map Creation with the Generic Mapping Tools (http://www.aquarius.geomar.de/omc/).

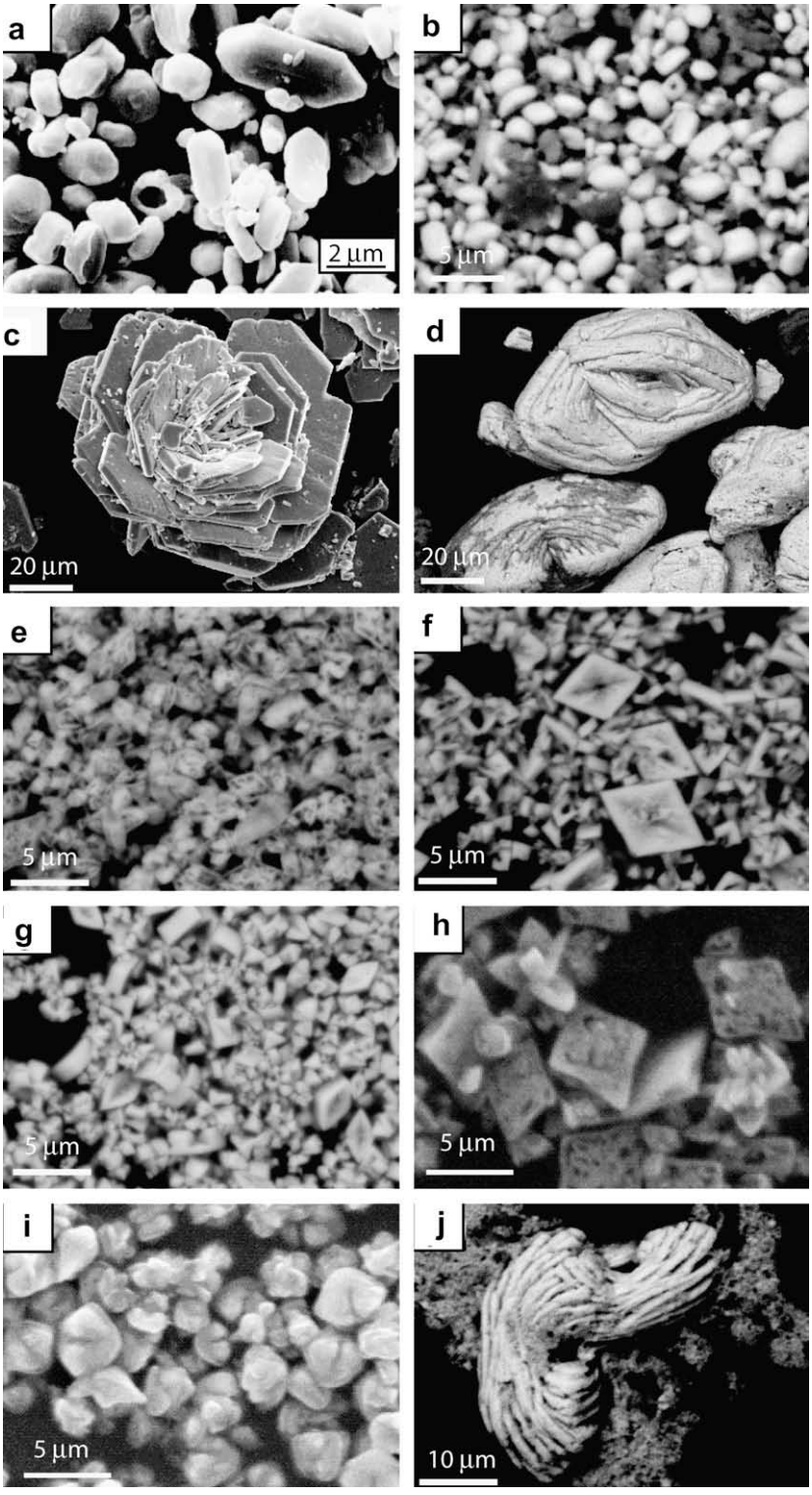

Fig. 2. Morphology of natural (a–d) and synthetic (e–j) barite crystals seen in scanning electron micrographs. Euhedral to sub-spherical marine barite, coretop sediments: (a) Pleiades expedition core 77, 1.03°N, 119.55°W, and (b) TN057-10 core, 47.09°S, 5.92°E. Cross-cutting tabular crystals and rosette structure of hydrothermal barite: (c) Guaymas Basin. Platy tabular cold seep barite: (d) San Clemente Sea Cliff 355. Rhombic to irregular crystals, synthetic barite: (e) Experiment 1A, (f) Experiment 1C, (g) Experiment 5C, (h) Experiment 2, and (i) Experiment 3. Synthetic barite agglomerate and fines: (j) Experiment 4. Images a, c, and h were taken in secondary electron mode. Images b, d–g, i, and j were taken in back scatter mode. Image (a) is adapted from Paytan et al. (2002).

Table 2
Summary of experiments conducted

Purpose:	Determine dependence of precipitation conditions on Ca-isotope fractionation														
Method:	Mix SO_4 and Ba solutions to precipitate $BaSO_4$ in the presence of Ca at different concentrations														
Name, solution chemistry	Temp. (°C)	SO_4 mmol/kg	Ba mmol/kg	Ca mmol/kg	Sat. Index[a]	a_{Ba}/a_{SO_4}	a_{Ca}/a_{Ba}	$\delta^{44/40}Ca_{solution}$	n[b]	$2\sigma_{mean}$[c]	$\delta^{44/40}Ca_{solid}$	n[b]	$2\sigma_{mean}$[c]	$\Delta^{44/40}Ca$	+/− [d]
Precipitation experiments															
1A, seawater+$BaCl_2$	5	29[e]	0.5	9	3.97	0.03	14.5	− 0.05	6	0.15	−3.28	4+(1)	0.36	−3.23	0.39
1B, seawater+$BaCl_2$	20	29[e]	0.5	9	3.71	0.03	14.3				−2.77	3	0.18	−2.72	0.23
duplicate	23	29[e]	0.5	9	3.66	0.03	14.3				−2.45	(2)	0.16	−2.40	0.22
1C, seawater+$BaCl_2$	40	29[e]	0.5	9	3.40	0.03	14.3				−2.62	4+(1)	0.42	−2.57	0.45
2, seawater+$CaCl_2$+$BaCl_2$	19	29[e]	0.5	13	3.72	0.03	20.8	−0.54	1+(1)	0.17	−3.45	3	0.19	−2.91	0.25
3, seawater+$CaCl_2$+$BaCl_2$	19	29[e]	0.5	72	3.65	0.04	111.1	−1.20	2+(1)	0.30	−4.62	1		−3.42	0.38
duplicate	21	29[e]	0.5	72	3.61	0.04	111.1				−4.43	3	0.50	−3.23	0.58
4, seawater+$BaCl_2$	21[f]	29[e]	0.02	9	2.30	0	333.3	−0.14	2	0.09	−2.78	2	0.17	−2.64	0.19
5A, MilliQ+$BaCl_2$+$CaCl_2$+$NaSO_4$	5	0.9	0.4	8	3.13	0.62	19.6	−0.85	2	0.14	−4.20	2	0.09	−3.35	0.17
5B, MilliQ+$BaCl_2$+$CaCl_2$+$NaSO_4$	21	0.8	0.4	8	2.82	0.73	19.6				−4.16	3	0.25	−3.31	0.29
5C, MilliQ+$BaCl_2$+$CaCl_2$+$NaSO_4$	40	1.3	0.4	8	2.74	0.46	19.2				−3.92	2	0.00	−3.07	0.14

[a] Initial saturation index (S.I.) calculated from the solution chemistry after addition of feed solution(s) using Visual MINTEQ 2.52. (Gustafsson, 2007).
[b] n = number of TIMS analyses on a single sample; numbers in parentheses were sample runs analyzed at IFM-GEOMAR.
[c] $2\sigma_{mean} = 2\sigma/n^{0.5}$ calculated from repeated TIMS measurements of an individual sample.
[d] Uncertainty of $\Delta^{44/40}Ca$ using error propagation.
[e] Approximate concentration in surface Pacific water.
[f] Fluctuations during length of experiment (~30 days) were approximately ±1 °C.

solutions (pH 5.5) that were added to seawater or Milli-Q water to induce barite precipitation (Table 2). All solutions were stirred continuously during experiments with a magnetic stirring rod. Experiments were conducted in acid cleaned glass beakers (1–20 L). Barite was collected after precipitation by filtration and rinsed with 8 M nitric acid and Milli-Q water, except Experiment 4 for which barite was not rinsed with nitric acid.

In all experiments, just enough feed solution was added to precipitate ~100 mg of barite, so that the solution Ca concentration was not significantly altered during the course of the precipitation experiments. Because we are ultimately interested in determining the effect of various parameters on Ca-isotope fractionation during incorporation into barite, it is important not to alter the concentration or isotopic composition of Ca in solution. To verify this, the concentration of Ca in solution was measured before and after each experiment using an inductively coupled plasma atomic-emission spectrometer (ICP-AES). A change of less than 10% in the Ca concentration was seen after each precipitation experiment except for Experiments 1A, 5A, and 5C, which showed changes of 13, 11, and 13% respectively. Some of this Ca could have precipitated out of solution as $CaSO_4$ that was subsequently removed from the sample when the precipitated barite was separated and rinsed before analysis.

The small change in solution Ca concentration ensures that the isotopic composition of the parent solution from which barite precipitates maintains a nearly constant isotopic signature (within analytical error) throughout the experiments. The $\delta^{44/40}Ca$ of solution in Experiment 1A (with the largest change in Ca concentration) was measured before and after barite precipitation and no significant isotopic change was detected. We suspect that this indicates some removal of Ca to phases (e.g. $CaSO_4$) other than barite in this experiment, because Rayleigh fractionation solely into barite would have changed the $\delta^{44/40}Ca$ of the residual solution by ~0.5‰ if all the Ca was incorporated into barite. A ~0.1‰ change (consistent with the observed insignificant difference) is easily explained by partitioning of Ca into a barite and $CaSO_4$ mixture. Since Experiment 1A represents the most Ca-depletion of any experimental solution, and no change in the $\delta^{44/40}Ca$ of the residual solution was detected, we assume that the isotopic composition of Ca in all other experimental solutions was likewise unaffected by barite precipitation.

In Experiment 1, 10 mM Ba solution was added gradually 1 mL at a time into 1 L of seawater at room temperature until ~100 mg of barite precipitated. In total 45 mL of 10 mM Ba (0.45 mmol Ba) was added over a period of approximately 10 min. The experiment was repeated at two additional temperatures (5 and 40 °C) and duplicated at room temperature (Table 2) to test the influence of changing temperature and initial saturation state on the isotopic fractionation of Ca in barite. Low temperature experiments (5 °C) were conducted in a cold room and high temperature experiments (40 °C) were conducted on a hot plate. In Experiments 2 and 3, filtered seawater was spiked with $CaCl_2$ to raise the Ca concentrations to 13 and 72 mmol/kg, to test the influence of Ca concentration on its isotopic fractionation during incorporation in barite. Ba was added following the method outlined for Experiment 1, to precipitate ~100 mg of barite at room temperature. In Experiment 4, a more dilute Ba solution (0.2 mM) was dripped into 20 L of filtered seawater at room temperature over approximately one month to test the influence of a low saturation state and $a{Ba^{2+}}/a{SO_4^{2-}}$. In total 0.45 mmol Ba was gradually added to 20 L of seawater (0.02 mM Ba).

In Experiment 5, $CaCl_2$ and $BaCl_2$ were added to ultrapure Milli-Q water to reach concentrations of 8 mmol/kg and 0.4 mmol/kg, respectively, nearly identical to conditions in Experiment 1. A total of 80–130 mL of 0.01 M SO_4 solution was then added to each beaker to induce barite precipitation (Table 2) over a period of approximately 10 min. The experiment was repeated at three different temperatures (5, 21, 40 °C). This experiment was designed to test the influence of different saturation states and solution chemistry (seawater vs. Milli-Q water).

In all experiments, barite precipitation occurred during addition of the feed solution to the precipitation medium after supersaturation was reached and continued until feed solution addition was complete. Precipitation rate was not measured. Crystal sizes varied among experiments (Fig. 2) but were not quantitatively determined. No general trend in crystal size was apparent in the experiments.

2.3.3. Saturation calculations

The saturation index (S.I.), defined as the difference between the log of the barium sulfate ionic product and the barite solubility product [log (IAP) − log(K_s)], was calculated for each experimental solution (Table 2) by the computer program Visual MINTEQ 2.52. (Gustafsson, 2007) from the solution chemistry after addition of feed solution(s), i.e. at initial precipitation conditions. The Davies method for activity correction was used with default databases, at the appropriate (fixed) pH, temperature, and ionic strength calculated from major ion concentrations (average seawater concentrations were used from Pilson, 1998). Ion activities in the experimental solution at initial precipitation conditions were also calculated by Visual MINTEQ 2.52 and reported in Table 2. Errors propagated by calculating the solution chemistry using this method are assumed to be identical for all experiments and should not significantly alter trends identified in the data. It is important to note that at the end of the experiments, no measurable Ba remained in solution for all experiments and no Ba or SO_4 remained after precipitation for Experiment 5. The desaturation of the solutions occurred over the time scale of the experiments (approximately 10 min) resulting from the precipitation of barite. The change in saturation during precipitation was roughly the same for each experiment and should not drastically affect our conclusions. Additional experiments should be done to investigate if variations in the desaturation of the solution during precipitation do in fact affect Ca-isotope fractionation.

2.3.4. Sample preparation

Pure barite samples (>95% barite) were dissolved by chelation with cation exchange resin (Mitsubishi Chemical

Industries, MCI Gel-CK08P) following Church (1970) and Paytan et al. (1993). The resin was cleaned prior to use with multiple rinses of distilled 8 M HCl and ultra-pure Milli-Q water and conditioned with water until the pH was ~5.5. 10 mg of barite sample was added to Teflon beakers with Milli-Q water and 1 mL of cleaned cation resin. The samples were heated in the oven to 90 °C for up to 10 days to dissolve the sample. Cations bind to the resin, separating from sulfate anions in solution. The anion-Milli-Q solution was decanted approximately daily and new Milli-Q water added. After dissolution, cations were extracted from the resin into an acid solution, using two separate rinses of 2 mL of ultra-pure 6 M HCl to ensure that all cations were released. Although complete dissolution of the barite was not always achieved, 100% of the Ca^{2+} in solution was recovered as determined using a standard solution similar to that expected for dissolved barite. Five marine barite samples were tested and no relationship was found between the measured Ca-isotope ratio of each sample and the difference between our dissolution step (yields of < 100%) and a dissolution procedure using a basic, ethylene diamine tetra acetic acid (EDTA) solution which yields 100% dissolution (Averyt and Paytan, 2003), see Fig. 3. This supports our assumption that the chelation dissolution step does not affect our measured Ca-isotope ratios.

2.3.5. Column chemistry and mass spectrometry

For the analysis of $^{44}Ca/^{40}Ca$ ratios in this study, we have used the widely accepted "double-spike" internal standard approach. Our double-spike, an artificially prepared Ca standard containing a precisely known excess of ^{42}Ca and ^{48}Ca, is added to the samples prior to chemical purification. The amount of spike added is adjusted to the Ca concentration of the sample so that a constant ratio of spike Ca to sample Ca is maintained between samples. In practice, in the resulting mixture greater than 90% of ^{40}Ca and ^{44}Ca are derived from the sample, while greater than 90% of ^{42}Ca and ^{48}Ca are derived from the double spike. Correction for fractionation and mathematical subtraction of the double-spike component from the mixture is accomplished using a widely accepted algorithm (Skulan et al., 1997). A constant ratio of spike Ca to sample Ca minimizes error propagation during data reduction but is not required by the algorithm. Small errors in measurement of sample calcium concentration do not significantly affect the quality of the data.

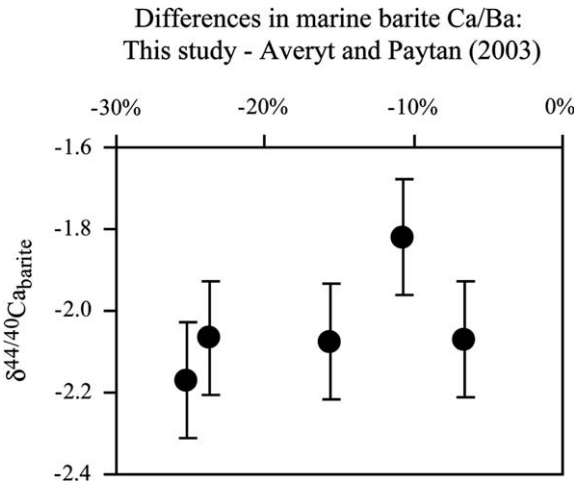

Fig. 3. Comparison of percent difference between estimated Ca/Ba from the chelation dissolution step (<100% yield) in this study and dissolution in a basic EDTA solution (100% yield; Averyt and Paytan, 2003) vs. the measured Ca-isotopic composition of marine barite. No significant relationship was found in Ca isotopes regardless of dissolution yield supporting the assumption that the chelation dissolution step does not affect our measured Ca-isotope ratios. Error bars are the average $2\sigma_{mean} = 0.14‰$.

Ca concentrations in the dissolved barite cation sample and precipitation solutions were determined using an ICP-AES. A sample aliquot of ~700 ng of Ca for each isotopic analysis was spiked using an internal standard of ^{48}Ca–^{42}Ca enriched solution (double-spike) of a precisely known Ca-isotope ratio to correct for isotopic fractionation occurring during the course of sample processing and analysis as discussed above. Samples were then evaporated to dryness, dissolved in 75 μL of 0.75 M HCl, and loaded onto small volume (1 mL) quartz columns filled with cation exchange resin (MCI Gel-CK08P) to separate Ca^{2+} from interfering cations (e.g. Sr^{2+}). Samples were eluted with ultrapure 1.8 M HCl and the purified Ca fraction was collected for analysis. Column blanks were less than 1% of the sample loaded on the column (less than 4 ng Ca). Full procedural blanks were less than 1% of total sample (less than 40 ng Ca). One synthetic barite sample was prepared three times and analyzed, indicating an external reproducibility of ±0.16‰ ($2\sigma_{mean}$).

Ca-isotope compositions were measured using a "double-spike" amendment technique on a Finnigan MAT 261 adjustable multi-collector thermal ionization mass spectrometer (TIMS) in multiple-collection dynamic mode at the U.S. Geological Survey at Menlo Park, California. Purified spiked Ca samples were re-dissolved in a small amount of H_3PO_4 and loaded onto single tantalum filaments (no activator was used). Current intensities for the ^{40}Ca ion beam were kept between 10–15 pA, and data was collected with a minimum of 60 isotope ratio measurements collected in blocks of 10 composite scans in a series of magnetic field-switched peak hops (first ^{40}Ca and ^{42}Ca were scanned simultaneously, then ^{42}Ca and ^{44}Ca simultaneously, then ^{48}Ca alone). Each measurement included a 4 s delay to allow the magnetic field to settle prior to ion current measurement for 4 s. Total time for analysis, including sample warm-up, is approximately 1.5 h. Ion currents were maintained at 1.0 to 1.5×10^{-11}A for the ^{40}Ca ion beam throughout an analysis, and beam focusing was rigorously optimized manually between each block of data collection. Internal precision of the algorithm-corrected $^{44}Ca/^{40}Ca$ ratio is typically better than 0.15‰ (2σ, 95% confidence). Double spike-subtracted $^{44}Ca/^{40}Ca$ ratios were normalized to the long-term average $^{44}Ca/^{40}Ca$ ratio determined for seawater on this mass spectrometer, in order to provide the basis for the "delta" scale reported in the data tables.

Replicates of the natural barite samples analyzed for this study yielded an average external (intra-assay) precision of ± 0.14‰ ($2\sigma_{mean}$). All but two samples were run in rep-

licate. External precision has been further assessed at the USGS lab over the past 4 years by running full procedural replicates on reference materials having $\delta^{44/40}$Ca values bracketing those of results presented here: ± 0.063‰ (2σ, 95% confidence) for 29 full procedural replicates of a seawater sample ($\delta^{44/40}$Ca=0‰); ± 0.040‰ for 90 replicates of La Jolla Ca ($\delta^{44/40}$Ca = −1.38‰); and ±0.154‰ for 10 replicates of NIST SRM915A ($\delta^{44/40}$Ca = −2.01‰). Additional details of the analytical procedures used for determination of Ca-isotope compositions and references to double-spike subtraction procedures and data validation techniques, are given in the Data Supplement of Skulan et al. (2007).

Several samples were also run on a Finnigan TRITON TIMS, using the same double-spike technique, at the IFM-GEOMAR research center in Kiel, Germany as indicated in Table 2. Complete details of the analytical method for the TIMS are outlined in Heuser et al. (2002). Comparing 18 calcite and barite samples run on both instruments (this study and Griffith et al., 2008), the interlab average absolute difference is 0.15‰, the root-mean-square difference is 0.20‰, and the mean difference (Kiel–Menlo Park) is 0.04‰. If we only consider barites measured in both labs (7 samples), δ^{44}Ca measured at Menlo Park is, on average, 0.22‰ lower than at Kiel. Although this might suggest that there is a small systematic offset between the two labs, it appears to be too small to affect any conclusions drawn from the present results. No interlaboratory correction has been applied to the data reported here.

For the hydrothermal and cold seep barite samples, Sr was also separated from all other cations following the same method described above for Ca and in Paytan et al. (1993). These samples were analyzed on the Finnigan MAT 261 TIMS adjustable collector instrument at the U.S. Geological Survey at Menlo Park, California following standard procedures as outlined in Bullen et al. (1996). ^{87}Sr/^{86}Sr measurements are precise within 2×10^{-5} (95% confidence level).

3. RESULTS

3.1. Theoretical equilibrium fractionation factors

3.1.1. Model crystal structures and vibrational (phonon) frequencies

Calculated unit cell parameters for calcite, barite, and both 25% and 12.5% mol. Ca-substituted barite are shown in Table 3. Model structures for calcite and barite conform closely to measurements (Graf, 1961; Jacobsen et al., 1998), generally slightly overestimating the size of each unit cell, and accurately reproducing measured atomic coordinates (RMS misfit 0.003 in fractional units). The tendency of plane-wave calculations, using gradient-corrected functionals like PBE, to overestimate unit cell volumes by ~3% is well known (e.g. Wu and Cohen, 2006).

Calculated frequencies of Raman and infrared-active vibrational modes (phonons) are compared with experiments in Fig. 4. It appears that the models slightly underestimate frequencies in barite, much like carbonate minerals, with an overall excellent correlation (RMS misfit ≈ 10 cm^{-1} after scaling by 1.052). However, in detail the best fit scale-factor for barite frequencies is slightly different than for calcite (1.052 vs. 1.032), a difference that exceeds the nominal statistical uncertainty in each scale factor. Since this study is concerned primarily with the difference between isotopic properties of these two crystals, we have chosen to use the calcite best-fit scale factor (1.032) for both crystals. This has the advantage of minimizing the effect of the empirical scale factor on calculated fractionations, and is also very close to the scale-factor previously used to estimate ^{13}C–^{18}O clumping equilibria, ^{13}C/^{12}C, and ^{18}O/^{16}O fractionation factors in carbonate minerals (Schauble et al., 2006). We will further test the effect of frequency scale factors below.

3.1.2. Estimated equilibrium ^{44}Ca/^{40}Ca fractionation factors

$\Delta^{44/40}$Ca is related to the fractionation factor (α) by the following equation (Criss, 1999):

$$\Delta^{44/40}\mathrm{Ca}_{\mathrm{A-B}} \approx 1000(\alpha_{\mathrm{A-B}} - 1) \approx 1000\ln(\alpha_{\mathrm{A-B}}) \quad (3)$$

For the present study, we have not been able to model dissolved Ca^{2+} directly, but we can calculate the fractionation between Ca-substituted barites and calcite, as shown in Fig. 5. The Ca-substituted barites are predicted to have much lower ^{44}Ca/^{40}Ca than calcite, by 8.9–9.4‰ at 0 °C and 7.5–7.9‰ at 25 °C. The 25% mol. and 12.5% mol. substituted barite models give very similar results (within ~0.6‰ over the temperature range of interest), consistent with the observation that the Ca–O coordination structures in these relatively Ca-rich barites are very similar. Based on the empirical potential models of large supercells, we expect that even sub-% Ca-substituted barite will show similar fractionation behavior. The predicted equilibrium barite-calcite fractionations overwhelm recently estimated calcite-water fractionations (Lemarchand et al., 2004; Fantle and DePaolo, 2007); strongly suggesting that barite will, at equilibrium, have much lower ^{44}Ca/^{40}Ca than a coexisting aqueous solution (e.g. by 6–8‰ at 25 °C). Apparently substitution of Ca^{2+} for the much larger Ba^{2+} ion leads to a weak bonding environment around Ca^{2+}, as discussed in more detail below.

The calculated temperature sensitivity of the barite-calcite fractionation is approximately 0.05‰ per °K (or °C) near ambient temperatures ($d[1000\ln(\alpha)]/dT \approx -2000\ln(\alpha)/T$, where T is in Kelvin). Polynomial fits of the calculated barite-calcite fractionation factors for 25% (Eq. 4a) and 12.5% (Eq. 4b) substituted barites as a function of absolute temperature are given below:

$$1000 \cdot \ln(\alpha_{\mathrm{Barite--calcite}}) = -6.92 \times 10^5/T^2 + 2.38 \times 10^9/T^4 \quad (4a)$$

$$1000 \cdot \ln(\alpha_{\mathrm{Barite--calcite}}) = -7.32 \times 10^5/T^2 + 2.42 \times 10^9/T^4 \quad (4b)$$

where T is in Kelvin. These fits reproduce calculated fractionation factors within 0.01‰ at temperatures above 263 K (−10 °C).

Table 3
Model crystal structures of calcite, barite, and ordered 25% and 12.5% Ca-substituted barite

Mineral, formula, and space group	Exp.[a]	Model	Mismatch
Calcite, $CaCO_3$, R–3c			
Unit cell			
$a = b = c$ (Å)	6.375	6.414	0.60%
*L*ab (°)	46.08	46.27	0.40%
Volume (Å^3)	122.65	125.75	2.50%
Atom positions (fractional)			
x_O	0.5078	0.5073	
Barite, $BaSO_4$, Pbnm			
Unit cell			
a (Å)	7.154	7.155	0.00%
b (Å)	8.879	8.819	−0.70%
c (Å)	5.454	5.513	1.10%
All angles 90°			
Volume (Å^3)	346.44	347.83	0.40%
Atom positions (fractional)			
x_{Ba}	0.1584	0.1554	
y_{Ba}	0.1845	0.1865	
x_S	0.1908	0.1873	
y_S	0.4375	0.4389	
x_{O1}	0.1072	0.1029	
y_{O1}	0.587	0.5925	
x_{O2}	0.0498	0.0437	
y_{O2}	0.3176	0.3157	
x_{O3}	0.3118	0.3096	
y_{O3}	0.4194	0.4209	
z_{O2}	0.9704	0.9714	
Ca: barite, $CaBa_3(SO_4)_4$, P1			
Unit cell			
a (Å)		7.1	
b (Å)		8.583	
c (Å)		5.518	
⟨bc (°)		90.07	
⟨ac (°)		91.13	
⟨ab (°)		88.16	
Volume (Å^3)		336.01	
Ca: barite, $CaBa_7(SO_4)_8$, P1			
Unit cell			
a (Å)		7.122	
b (Å)		8.676	
c (Å)		11.041	
⟨bc (°)		90.00	
⟨ac (°)		90.00	
⟨ab (°)		90.82	
Volume (Å^3)		682.19	

[a] Experimental or measured structure for calcite from Graf (1961) and barite from Jacobsen et al. (1998).

3.1.3. Accuracy of theoretical estimates

The first-principles calculations reported here are clearly somewhat crude, particularly in making a highly simplified treatment of Ca-substitution into the barite structure. It is not definitely known whether Ca substitutes into vacant Ba sites in barite, and the optimization procedure used here may have converged to a meta-stable structural configuration. The absence of imaginary phonon frequencies for at least two phonon wave vectors in each of the Ca-substituted barite models strongly suggests that they represent local energetic minima, but cannot guarantee that the global minima for Ca-defects have been found.

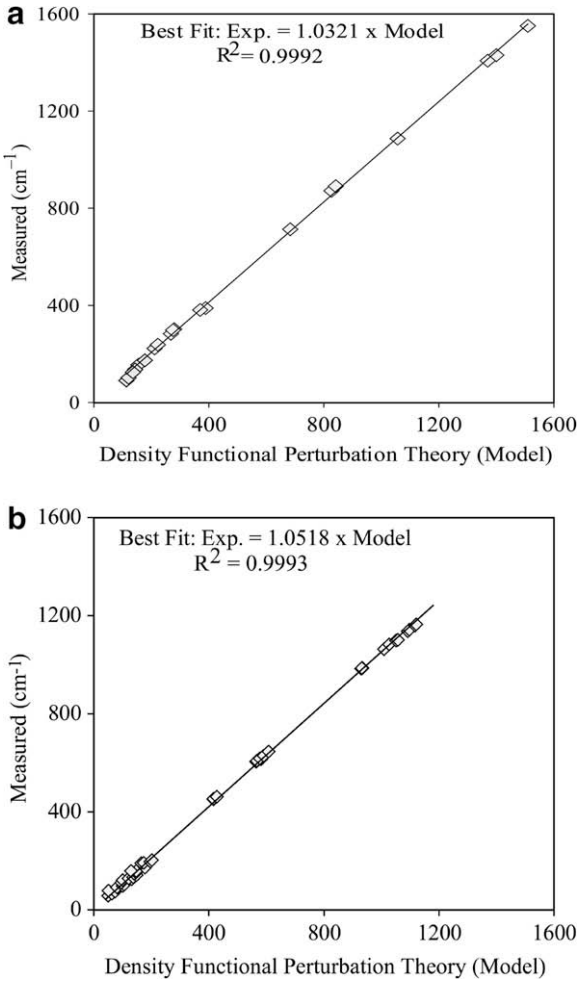

Fig. 4. Comparison of calculated phonon (vibrational) frequencies in (a) calcite and (b) pure barite with Raman and infrared measurements. Calcite measurements are from Porto (1966), Rutt and Nicola (1974) and Hellwege et al. (1977), with one additional datum from a neutron-scattering study by Cowley and Pant (1973). Barite data are from Dawson et al. (1977). Frequencies are indicated in wavenumber units (cm^{-1}).

Despite these uncertainties, our prediction of low $^{44}Ca/^{40}Ca$ in barite is consistent with the expected crystal-chemistry of Ca^{2+}–Ba^{2+} substitution. The Ca^{2+} ion (1.12 Å in 8-fold coordination; Shannon, 1976) is considerably smaller than Ba^{2+} (1.42 Å in 8-fold coordination), suggesting that the Ca–O bonds in barite are strained. In fact, the eight shortest Ca–O bonds in the optimized substituted barite structures average 2.60–2.67 Å, much longer than the average Ca–O bond length (2.47 Å) in $CaSO_4$-anhydrite (Hawthorne and Ferguson, 1975). In addition, Ca occupies a more compact 6-fold (octahedral) coordination site in calcite, with even shorter Ca–O bond lengths (2.36 Å; Graf, 1961) and higher-order Ca–O bonds. Bond stretching and increased coordination number both will tend to decrease the force constants acting on the Ca^{2+} ion in barite, relative to calcite, reducing the relative affinity of the barite cation

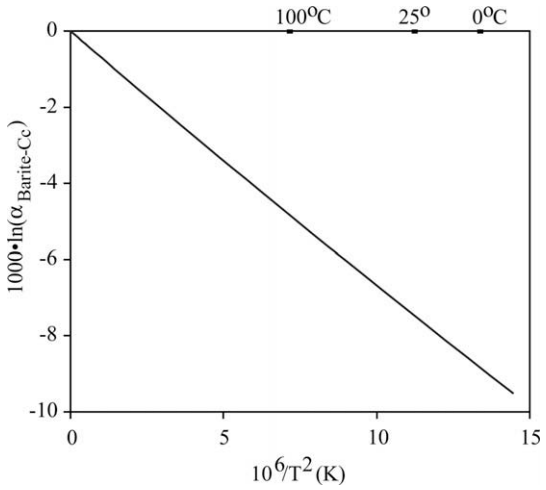

Fig. 5. Theoretical equilibrium $^{44}Ca/^{40}Ca$ fractionation between 25% calcium-substituted barite and calcite, $1000\ln(\alpha_{Barite-Cc})$.

site for heavy Ca-isotopes. The unusually long, weak Ca–O bonds in barite probably cause the extreme isotopic fractionation predicted by the first-principles models. The coordination structure of un-complexed Ca in solution is thought to be 6- to 8-fold (e.g. Bakó et al., 2002; Fulton et al., 2003; Bruneval et al., 2007), and the Ca–O (solvation) bonds are unlikely to be strained in such an easily deformed medium (observed mean bond length ~2.4 Å), so it is also reasonable to expect much lower $^{44}Ca/^{40}Ca$ in barite in equilibrium with an aqueous solution.

Compared to uncertainties stemming from the simplified treatment of Ca-substitution into the barite structure, other errors in the first-principles calculations are likely to be minor. Changing the frequency scale factor for barite from 1.032 to the barite best-fit value of 1.052 changes the calculated fractionation factors by only ~0.2‰ at 0–25 °C, slightly increasing the estimated $^{44}Ca/^{40}Ca$ of barite. Eliminating the scale factors entirely for both calcite and barite will change the estimated fractionation factors by 0.4–0.5‰ over the same temperature range. Estimates of likely anharmonic effects and imperfect correlation between model and measured phonon frequencies suggest a total uncertainty of approximately ±1‰, but the error could be much larger if Ca-substitution into barite is mischaracterized by the model.

3.2. Natural barite

3.2.1. Marine barite

The average $\delta^{44/40}Ca$ of Holocene coretop marine (pelagic) barite in the modern oceans is −2.01‰ ± 0.15 (average $2\sigma_{mean}$) as determined from measurements of 23 samples from 15 locations (Table 4, Fig. 6). These samples are much less depleted in ^{44}Ca than predicted by our model of equilibrium fractionation, suggesting a kinetic fractionation mechanism. No clear relationship exists between the Ca-isotope composition of marine barite and the average annual temperature (1–14 °C) in the upper 700 m of the water column (Fig. 7a), where the majority of marine barite is thought to precipitate (Chow and Goldberg, 1960; Dehairs et al., 1980; Bishop, 1988; Stroobants et al., 1991). There is also no detectable correlation with the depth of coretop locations, ranging from 3175–4431 m (Fig. 7b). No relationship is observed between the Ca-isotope composition of marine barites and the sampled ocean basin, the dominant organism, bulk sediment and barite accumulation rates, the water column barite saturation (at the seafloor or 700 m), and other upper (700 m) water column properties such as salinity, carbonate concentration, and dissolved oxygen concentration (data not shown).

It has been shown that marine barite directly records the $^{87}Sr/^{86}Sr$ of contemporaneous seawater (Paytan et al., 1993) and therefore its Sr source is most likely seawater or a Sr source identical to seawater such as marine biogenic carbonates. If Ca has the same source as Sr during marine barite precipitation, the Ca-isotope composition of the parent solution could either be the same as seawater, or possibly be controlled by Ca derived from marine biogenic matter such as dissolved carbonate tests. These two pools of Ca probably have different Ca-isotope compositions: seawater $\delta^{44/40}Ca$=0.00‰ and average marine carbonate $\delta^{44/40}Ca \approx -1.2$‰ (e.g. Heuser et al., 2005). Evidence for the origin of the Ca in barite comes from the homogenous isotopic composition of measured marine barite samples (± 0.15‰). We believe it is unlikely, although possible, that the contribution of Ca from degrading and dissolving biogenic matter within the microenvironments in which marine barite precipitates is identical throughout all ocean basins. Therefore, we conclude that the dominant source of Ca in marine barite is probably seawater, which has a uniform Ca-isotope composition at any given time in the ocean due to its long residence time of ~1 million years (Broecker and Peng, 1982). This indicates an apparent effective fractionation between marine barite and its parent solution (seawater) of − 2.01‰ (± 0.15‰).

3.2.2. Hydrothermal and cold seep barite

Hydrothermal and cold seep barite samples record lower $\delta^{44/40}Ca$ values than marine barite (i.e. light isotope enrichment) and exhibit a range of Ca-isotope compositions from −4.13‰ to −2.72‰ (Table 4, Fig. 6). Thus it appears that the measured hydrothermal and cold seep barite samples are isotopically distinct from Holocene marine barite (−2.01‰). However, these natural samples are also, like marine barite, significantly less depleted in ^{44}Ca than predicted by our equilibrium models, suggesting they also did not precipitate in equilibrium with seawater, hydrothermal, or cold seep fluids.

The Ca sources (parent solutions) during barite precipitation in these natural settings include several potential end members: hydrothermal fluids ($\delta^{44/40}Ca \approx -0.96$‰; Schmitt et al., 2003a; Amini et al., 2008), seawater ($\delta^{44/40}Ca$=0.00‰; Hippler et al., 2003), and cold seep fluids which include a range of Ca-isotope signatures, i.e. a mixture of Ca from seawater, brines, carbonates, sulfates, or silicates (Teichert et al., 2005). In order to determine the empirical fractionation between solid and solution (Eq. 2), the Ca-isotope composition of the solutions from which the natural barite samples precipitated must be defined.

Table 4
Summary of natural barite results

Name	Latitude	Longitude	Depth (mbsl)	Temp. [a] (°C)	$\delta^{44/40}Ca$	Samples	n[b]	$2\sigma_{mean}$[c]	$^{87}Sr/^{86}Sr$[d]	Sediment description
Holocene marine (pelagic) barite										
Polarstern—PS2499-1	46.5°S	15.3°W	−3175	4	−1.88	1	2	0.07		Calcareous ooze with siliceous component
T. Thompson—TNO57-10	47.1°S	5.9°E	−4398	3	−2.15	2	2	0.05		Siliceous ooze with clay, foraminifera bearing
Pleiades—PLDS-069PG	1.0°N	105.6°W	−3527	11	−2.06	4	8	0.09		Calcareous, biogenic, sandy mud
Pleiades—PLDS-070Bx	1.1°N	107.2°W	−3694	11	−1.82	2	4	0.08	0.70918	Calcareous, biogenic, sandy mud
Pleiades—PLDS-077Bx	1.1°N	119.9°W	−4366	12	−2.07	1	2	0.18	0.70917	Calcareous, biogenic, sandy mud
JGOFS TTN013_58	0.1°N	139.7°W	−4301	12	−2.15	1	3	0.39		Calcareous biogenic ooze
JGOFS TTN013_82	2.0°N	140.2°W	−4413	13	−2.07	2	6	0.05		Calcareous biogenic ooze
JGOFS TTN013_88	0.8°N	139.9°W	−4415	12	−2.06	1	3	0.25		Calcareous biogenic ooze
JGOFS TTN013_113	4.0°N	139.9°W	−4431	12	−1.94	3	6	0.19		Calcareous biogenic ooze
Venture01—VNTR01-5GC	2.8°N	110.6°W	−3764	12	−1.91	1	2	0.14		Terrigenous mud, foraminifera bearing
Venture01—VNTR01-8PC	0.0°N	110.5°W	−3791	11	−2.05	1	2	0.14		Calcareous, foraminifera, sandy mud
Venture01—VNTR01-10GC	4.5°S	102.0°W	−3405	11	−2.21	1	2	0.10		Calcareous, foraminifera, sandy mud
Venture01—VNTR01-11GC	0.1°N	95.3 °W	−3345	11	−2.01	1	2	0.23		Calcareous, foraminifera, sandy mud
Nathaniel B. Palmer—NBP9802 7MC2	66.1°S	169.5°W	−3995	1	−2.07	1	1			Diatomaceous, carbonate ooze, ice rafted debris
Eurydice—ERDC-125	0.0°S	161.0°E	−3368	14	−1.73	1	2	0.14	0.70918	Calcareous, biogenic mud or ooze, sandy
Cold seep barite										
San Clemente Basin	32°N	117.5°W	−1800		−2.72	1	2	0.15	0.70866	Stratiform, bedded barite
Baja California, Ensenada	31.5°N	116.5°W			−3.31	1	2	0.23	0.70878	Massive barite
Hydrothermal barite										
Guaymas Basin	27°N	111.5°W	−2000		−2.74	2	3	0.02	0.70595	Massive barite
MidAtlantic Ridge	26°N	44.5°W	−3500		−3.15	1	2	0.06	0.70516	Barite mounds and chimneys
JdFR ALV 2254-22 ext. chim. Mid. Valley	48°N	128.5 °W	−2400		−3.42	1	2	0.10	0.70442	Barite mounds and chimneys
JdFR ALV 2254-22 int. chim. Mid. Valley	48°N	128.5°W	−2400		−3.99	1	2	0.41	0.70443	Barite mounds and chimneys

[a] Average temperature in the upper 700 m of the water column from World Ocean Atlas 1998 (Conkright et al., 1998).
[b] n=number of TIMS analyses on a single sample.
[c] $2\sigma_{mean}=2\sigma/n^{0.5}$ calculated from repeated TIMS measurements of an individual sample.
[d] Marine barite results from Paytan et al. (1993).

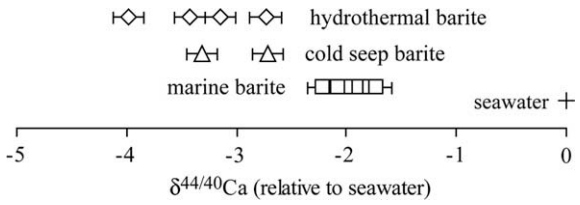

Fig. 6. Natural barite results. Error bars are the average $2\sigma_{mean} = 0.14‰$.

Therefore, the $^{87}Sr/^{86}Sr$ of each sample was also measured (Table 4) because it has been useful in previous studies to distinguish between potential sources of Sr^{2+} during barite precipitation (e.g. seawater or hydrothermal fluids; Paytan et al., 2002) and might reveal similar information about the source of Ca^{2+}.

Hydrothermal barite samples precipitate where hydrothermal fluids and seawater mix. We estimated the Ca-isotope composition of the hydrothermal fluid using the calculated ratio of hydrothermal to seawater determined by $^{87/86}Sr$ for hydrothermal barite samples (see Paytan, 1996; Paytan et al., 2002). This calculation is based on the assumptions that Ca concentrations of the solutions are the same (seawater is ~10.3 mmol/kg and estimates range from 10.5 to 55 mmol/kg for hydrothermal fluid; Elderfield and Schultz, 1996), the isotopic composition of seawater is 0‰ (Hippler et al., 2003), and the effective fractionation factor during barite precipitation is equal to that for marine pelagic barite. The calculated range of values is large, −1.28 to −2.36‰, and significantly less enriched in ^{44}Ca than the expected end-member value of hydrothermal fluid (−0.96‰; Schmitt et al., 2003a; Amini et al., 2008). It is possible that either (1) the Ca-isotope composition of the hydrothermal fluids from which barite precipitates varies depending on the water-rock ratio, anhydrite precipitation, or phase separation processes within the hydrothermal environment (Amini et al., 2008) and/or (2) the assumed fractionation factor is not the same as for marine barite and varies depending on the precipitation environment for the hydrothermal barite. If we assume the isotopic composition of hydrothermal fluid is −0.96‰, the calculated fractionation, $\Delta^{44/40}Ca$, for the measured hydrothermal barite varies between −2.19 and −3.18‰. This is significantly different from marine barite, $\Delta^{44/40}Ca = -2.01‰$.

Cold seep barite samples have $^{87}Sr/^{86}Sr$ values lower than seawater and marine barite, but higher than hydrothermal barite (Table 4). Because cold seep fluids are likely a mixture of many sources of Ca^{2+} (e.g. seawater, brines, carbonates, sulfates, or silicates), it is not possible to determine precisely the $\Delta^{44/40}Ca$ or isotopic fractionation of these samples.

3.3. Synthetic barite

Ca-isotopes in synthetic barite, like hydrothermal and cold seep samples, are more depleted in the heavy Ca-isotopes (lower $\delta^{44/40}Ca$ values), and span a larger range (~1‰) of Ca-isotope compositions than marine barite, $\Delta^{44/40}Ca = -3.42$ to −2.40‰ (Table 2). These values are isotopically distinct from Holocene marine barite, but overlap the range of hydrothermal and cold seep barites that were measured. Interestingly, the synthetic samples are not as strongly depleted in ^{44}Ca as predicted by our equilibrium model. Thus all of the natural and synthetic barites appear to show kinetically-controlled Ca-isotope fractionations resulting in an offset from equilibrium values (Figs. 6 and 8).

In Experiment 1, all conditions were kept near constant except temperature, which was varied from 5 to 40° C, resulting in a 15% decrease in saturation index (S.I.) from 3.97 to 3.40. At high saturation states (low temperatures), the barite was more fractionated from the solution than at lower saturation states (higher temperatures) (Fig. 9a). The measured temperature shift corresponds to approximately +0.02‰ per °C, or ~1‰ per S.I. unit. If the change in fractionation is truly a temperature effect, it is similar in magnitude to (but somewhat smaller than) the equilibrium

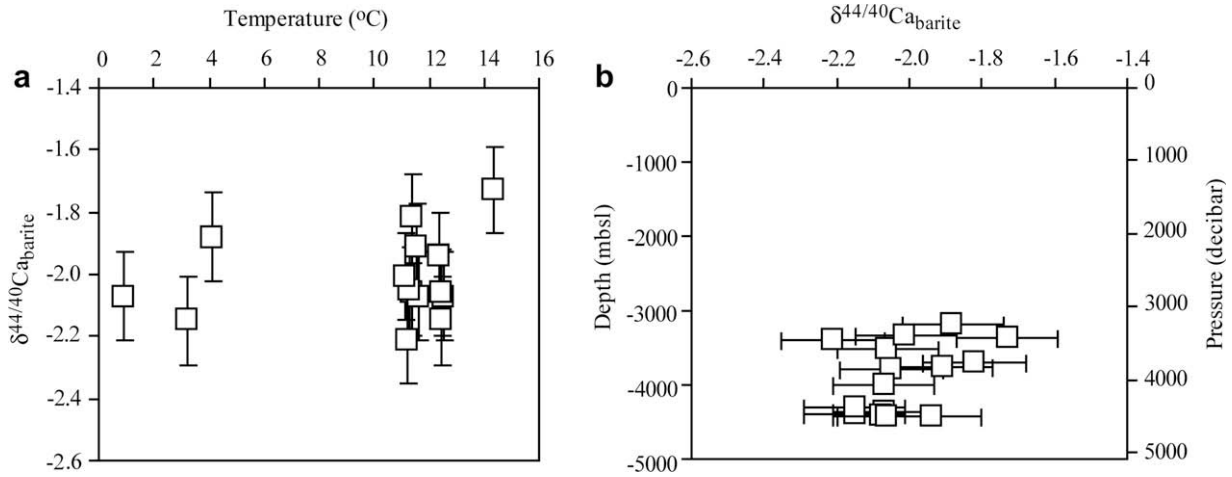

Fig. 7. Holocene marine (pelagic) barite Ca isotopes vs. (a) average temperature in upper 700 m of water column (Conkright et al., 1998) and (b) depth of coretop (meters below sea level) and approximate pressure at the seafloor (calculated at salinity = 35 and temperature = 0°C). Error bars are the average $2\sigma_{mean} = 0.14‰$.

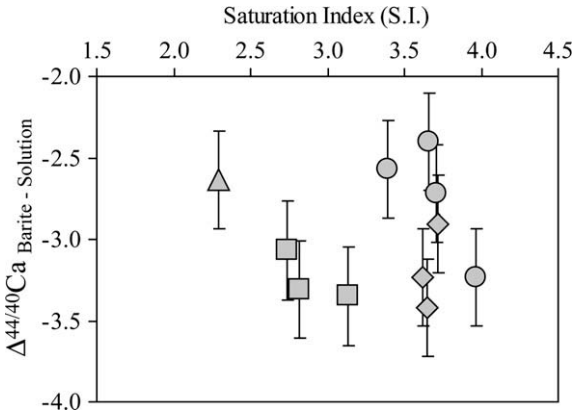

Fig. 8. Synthetic barite results. $\Delta^{44/40}Ca_{Barite\text{-}solution}$ vs. Saturation Index (S.I.). Symbols include Experiment 1 (circles), Experiment 2 and 3 (diamonds), Experiment 4 (triangle), and Experiment 5 (squares). Error bars are the average uncertainty = 0.30‰ for the experiments.

temperature dependent fractionation, calculated to be approximately +0.05‰ per °C. However it is not possible to identify whether this is a temperature and/or saturation state effect as these varied together in our experiments.

It appears that an increase in the ratio of $a\mathrm{Ba}^{2+}/a\mathrm{SO_4}^{2-}$ or a decrease in the $a\mathrm{SO_4}^{2-}$ results in an increase in the fractionation of Ca-isotopes (lower $\Delta^{44/40}$Ca values), when comparing Experiments 1B to 2B and Experiment 1A to 2C with all other parameters held nearly constant (Table 2). However, these results do not eliminate the possibility that these changes are due solely to the variations in $a\mathrm{SO_4}^{2-}$, since $a\mathrm{Ba}^{2+}$ was similar in these experiments.

The ratio of $a\mathrm{Ca}^{2+}/a\mathrm{Ba}^{2+}$ also appears to influence the isotopic fractionation of Ca^{2+} incorporated into barite during precipitation. Barite in Experiments 1B, 2, and 3 were precipitated under identical $a\mathrm{SO_4}^{2-}$, $a\mathrm{Ba}^{2+}/a\mathrm{SO_4}^{2-}$, temperature, and saturation conditions, but a range of Ca concentrations resulting in more than a sevenfold increase in the ratio of $a\mathrm{Ca}^{2+}/a\mathrm{Ba}^{2+}$ (from 14 to 111). An decrease in the ratio of $a\mathrm{Ca}^{2+}/a\mathrm{Ba}^{2+}$ (or decrease in $a\mathrm{Ca}^{2+}$ with $a\mathrm{Ba}^{2+}$ held constant) resulted in less fractionation of Ca^{2+} during incorporation into barite (Fig. 9b). However, it is not possible to identify whether this is an effect due to a change in Ca concentration or $a\mathrm{Ca}^{2+}/a\mathrm{Ba}^{2+}$. Measuring the Ca:Ba ratio of the barite samples (Averyt and Paytan, 2003) could give additional insight on the fractionation process related to this parameter and to determine if chemical equilibrium was achieved.

4. DISCUSSION

4.1. Application of predicted equilibrium fractionations

As demonstrated in our theoretical equilibrium fractionation models, barite is expected to be ^{44}Ca-poor relative to the solutions from which it precipitated, and ^{44}Ca-poor relative to other minerals such as calcite, aragonite (e.g. Gussone et al., 2005), apatite (Schmitt et al., 2003b), gypsum, and anhydrite (Hensley, 2006). This is supported by the measured natural and synthetic samples (Fig. 6). Isotopic fractionation is also expected to decrease with an increase in temperature in a system at equilibrium (Bigeleisen and Mayer, 1947; Urey, 1947) as shown in Fig. 5 for Ca-substituted barite and calcite.

If the equilibrium isotopic fractionation factor is reasonably well described by our theoretical model, none of the measured barite samples appear to be in isotopic equilibrium with calcite, seawater, or plausible hydrothermal and experimental fluids. We calculate that at 25 °C, the equilibrium $\Delta^{44/40}Ca_{Barite\text{–}calcite}$ is −8‰. Measured barites indicate $\Delta^{44/40}Ca_{Barite\text{–}calcite}$ of approximately −3‰ ± 1‰, assuming an equilibrium calcite-solution fractionation of 0‰ (Fantle and DePaolo, 2007), or $\Delta^{44/40}Ca_{Barite\text{–}calcite}$ of approximately −1.5‰ ± 2‰, assuming an equilibrium calcite-solution fractionation of −1.5‰ (Lemarchand et al., 2004). Although the measured fractionations have the same sign as the theoretical model, i.e. barites have lower $\delta^{44/40}$Ca values than the solutions from which they precipitate, the implied magnitude of $\Delta^{44/40}Ca_{Barite\text{–}calcite}$ is much less than that predicted by our theoretical equilibrium model.

This could be explained using a model of Ca-isotope fractionation originally constructed to explain fractionation in inorganic calcite by Lemarchand et al. (2004). In their model, kinetic processes increase the amount of Ca^{2+} precipitated in the crystal outside of an "equilibrium zone"

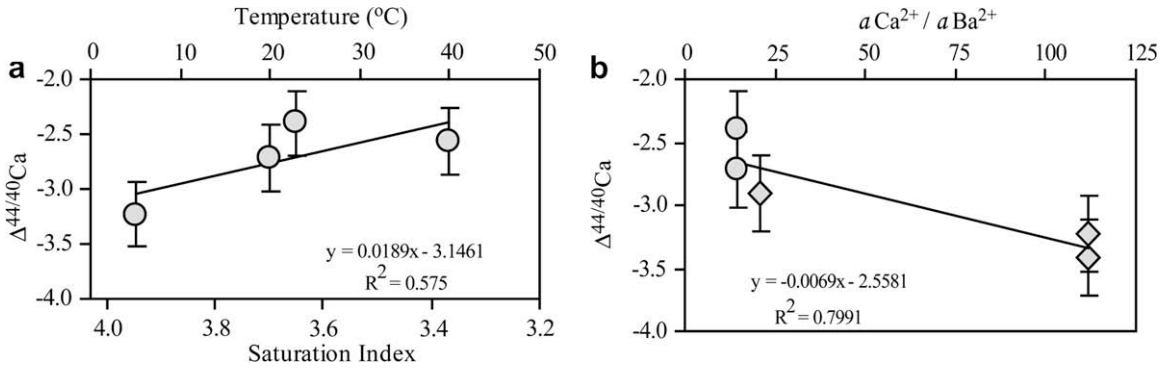

Fig. 9. $\Delta^{44/40}Ca_{Barite\text{-}solution}$ of synthetic barite in permil vs. (a) temperature for Experiment 1 (circles) and (b) $a\mathrm{Ca}^{2+}/a\mathrm{Ba}^{2+}$ for Experiments 1B (circles), 2 and 3 (diamonds). Error bars are the average uncertainty = 0.30‰ for the experiments.

(where the crystal surface is in isotopic equilibrium with the solution), decreasing the observed fractionation relative to the equilibrium effect. In their experiments, the dominant kinetic process was related to oversaturation of a region of the crystal surface-solution boundary layer. The resulting isotopic shifts were interpreted to be a mixture of the equilibrium isotope value with the bulk isotopic composition of the solution (Lemarchand et al., 2004). Similarly, the direction of Ca-isotope fractionation in natural and synthetic barites measured in this study appears to be governed by equilibrium isotope fractionation (calculated by the theoretical model) that is influenced to various degrees by one or more kinetic processes under different precipitation conditions.

During barite precipitation, several processes control trace metal incorporation and distribution in the crystal structure, which collectively appear to affect the observed Ca-isotope fractionation. Kowacz et al. (2007) showed that growth modes and rates of barite precipitation change as the cation/anion activity ratio ($a\mathrm{Ba}^{2+}/a\mathrm{SO_4}^{2-}$) changes, potentially influencing Ca-isotope fractionation. Because Ca is a trace component of barite, parameters affecting Ca^{2+} substitution for Ba^{2+}, such as $a\mathrm{Ca}^{2+}/a\mathrm{Ba}^{2+}$, also may be quite important, although this is not a major consideration for Ca-isotope fractionation during precipitation of a mineral in which Ca^{2+} is the major cation, e.g. calcite or aragonite. These processes will be discussed further in the following sections.

4.2. Interpreting observed fractionations, $\Delta^{44/40}$Ca in barite

4.2.1. Fractionations, $\Delta^{44/40}$Ca in natural samples

The general observation is that Ca-isotopes in marine pelagic barite are less fractionated from their parent solution (seawater) than other natural barite samples (and synthetic barite samples). Marine barite precipitates within microenvironments in seawater with low saturation states (saturation below or near equilibrium, S.I. ≈ 0; Monnin et al., 1999; Monnin and Cividini, 2006) and seemingly slow precipitation rates (Ganeshram et al., 2003). This is in contrast to the conditions within fluids from which other natural barites most likely precipitate, which have Ba concentrations much higher than seawater (Elderfield and Schultz, 1996). Without knowing the precise precipitation rate, we can only infer that the precipitation rate of marine barite is less than that of other natural barites and synthetic barite samples in this study. These results therefore suggest a positive rate dependence of Ca-isotope fractionation when comparing marine barite to the other measured barite samples, such that increased Ca fractionation occurs at higher precipitation rates. These results imply that kinetic isotope effects related to precipitation rate are less pronounced in marine barite than in the other barite samples. Therefore marine barite could actually have less kinetic isotope effects than the other measured samples even though its isotope ratio is further from the calculated equilibrium value.

The precise relationship between Ca-isotope fractionation in barite and precipitation rate appears to be more complicated when considering all inferred rate-relationships (e.g. between marine barite and synthetic barite or between synthetic barites). This is not surprising given recent results suggesting a complex relationship between Ca-isotope fractionation and precipitation rate in $CaCO_3$ (Fantle and DePaolo, 2007; Tang et al., 2008).

Marine barite does not appear to be as strongly affected by other kinetic processes that fractionate Ca^{2+} during incorporation as the other natural and synthetic barites measured in this study (see discussion in following section). Most important for paleoceanographic applications, Ca-isotope fractionation in marine barite is not measurably affected by the range of environmental conditions in the modern ocean measured in this study including temperature (1–14 °C), salinity (34.2–34.9), water column barite saturation ($\Omega = 0.6$-1.2), carbonate concentration (86–126 μmol/kg), dissolved oxygen concentration (1–6 ml/L) or sedimentation and barite accumulation rates (1.7–2.7 cm/kyr, 0.1–2.3 μg/cm^2/yr, respectively).

4.2.2. Fractionations, $\Delta^{44/40}$Ca in synthetic barite

If the measured $\Delta^{44/40}$Ca (and α) was constant in our experiments, then it could be interpreted as the equilibrium fractionation factor without any measurable kinetic effects. However, when comparing the isotopic composition of barite precipitated at room temperature to the isotopic composition of dissolved Ca^{2+} in the precipitation solution, the experiments do not all fall on a constant fractionation line (Fig. 10). Differences in $\Delta^{44/40}$Ca (and α) between precipitation experiments likely result from kinetic isotope effects including saturation state effects related to precipitation rate as described in the previous section.

Similar to published inorganic calcite precipitation experiments (Lemarchand et al., 2004), our results show that the dominant controlling parameter for fractionation of Ca-isotopes is not only the degree of supersaturation (Fig. 8), but also other physicochemical conditions during precipitation (e.g. temperature, elemental concentrations).

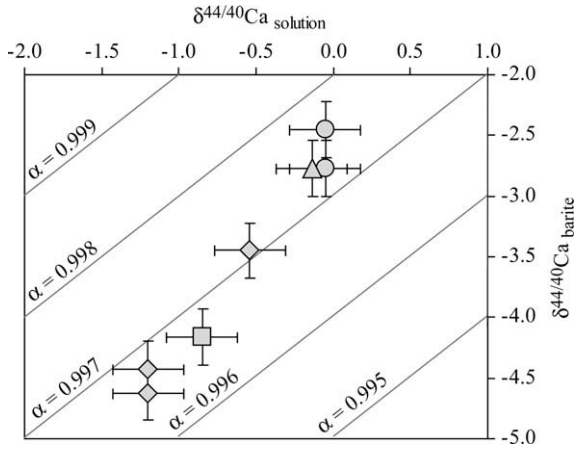

Fig. 10. Synthetic barite results for room temperature experiments. Isotopic composition of precipitated barite versus the isotopic composition of dissolved Ca^{2+} in the precipitation solution. Symbols include Experiment 1 (circles), Experiment 2 and 3 (diamonds), Experiment 4 (triangle), and Experiment 5 (squares). Hypothetical fractionation factors between solid (barite) and solution ($\alpha_{\text{solid-solution}}$) are given and plotted (gray lines). Error bars are the average $2\sigma_{\text{mean}} = 0.23‰$ for the experiments.

All experiments were preformed with $[SO_4^{2-}]$ in excess with respect to $[Ba^{2+}]$ because this is most similar to natural conditions in the modern ocean. When $[SO_4^{2-}]$ is in excess with respect to $[Ba^{2+}]$, it is thought that desolvation of the cation (Ba^{2+} or Ca^{2+}) at the crystal surface is the rate limiting kinetic process for two-dimensional nucleation and crystal growth (for solutions with S.I. between 0.86 and 1.1; Kowacz et al., 2007). If this holds for our experiments (with S.I. = 2.30–3.97), then aBa^{2+} and the ratio of aBa^{2+}/SO_4^{2-} should influence crystal nucleation and growth in addition to the saturation state. This suggests that an increase in nucleation and/or growth rate of precipitating barite caused by an increase in the ratio of aBa^{2+}/SO_4^{2-} can increase the Ca-isotope fractionation in barite.

Our results support this hypothesis. There is a positive relationship between the degree of Ca-isotope fractionation and parameters that control precipitation mechanisms and/or rate, such as the saturation state and aBa^{2+}/aSO_4^{2-}, indicating that these factors likely control kinetic isotope effects. In contrast, Holocene marine barite samples have a constant offset from seawater and are not affected, within current analytical precision, by any known environmental factors.

The relative abundance of Ba^{2+} and Ca^{2+} in the precipitation solution could also contribute to the observed fractionation effects. The ratio of aCa^{2+}/aBa^{2+} could influence the diffusive transport of Ca^{2+} in the vicinity of the crystal/solution interface or within the first layers of the growing crystal. In our experiments, a positive relationship is found between aCa^{2+}/aBa^{2+} and the degree of Ca-isotope fractionation such that an increase in the relative abundance of Ca to Ba results in increased fractionation between Ca in barite and that in the bulk solution. This could occur because of (1) increased influence of the differences in the diffusive transport rate of ^{40}Ca relative to ^{44}Ca at higher aCa^{2+}/aBa^{2+} or, alternatively, (2) decreased influence of differences in the diffusive transport of ^{40}Ca relative to ^{44}Ca at higher aCa^{2+}/aBa^{2+} which allows the precipitated barite to approach closer to equilibrium isotope values (lower values). These experiments cannot differentiate between these two hypotheses.

5. CONCLUSION

Holocene marine barite samples from oxic, non-sulfate-reducing pelagic sediments in the major ocean basins are isotopically homogenous ($\delta^{44/40}Ca = -2.01 \pm 0.15‰$) and distinct from other types of barite ($\delta^{44/40}Ca = -4.13$ to $-2.72‰$). Thus the Ca-isotope composition of pristine marine (pelagic) barite is a promising recorder of seawater Ca-isotope composition through time, with a constant offset from seawater of $-2.01 \pm 0.15‰$. Laboratory precipitated (synthetic) barite samples, like hydrothermal and cold seep samples, are more depleted in the heavy Ca-isotopes than marine barite and span a large range of Ca-isotope compositions, $\Delta^{44/40}Ca = -3.42$ to $-2.40‰$.

First-principles lattice dynamical models predict that barite will have much lower $^{44}Ca/^{40}Ca$ in equilibrium with calcite, by $-9‰$ at 0 °C and $-8‰$ at 25 °C. If the equilibrium isotopic fractionation factor is best described by this model, none of the measured barite samples appear to be in isotopic equilibrium with calcite. Although the measured results have the same sign as the theoretical model, the magnitude of Ca-isotope fractionation is less in our measured samples compared to the theoretical equilibrium model. It seems that kinetic fractionation processes must therefore control the extent to which the mineral equilibrium fractionation is exhibited under the precipitation conditions for the measured samples. Potential fractionation mechanisms include processes influencing Ca-substitution for barium in barite, nucleation, and crystal growth. When appropriate experiments were compared to isolate specific parameters that may impact the $\Delta^{44/40}Ca$ (e.g. temperature, saturation state, aBa^{2+}/aSO_4^{2-}, and aCa^{2+}/aBa^{2+}), our results indicate that factors related to precipitation mechanisms and rate can affect the fractionation of Ca-isotopes in barite. Further work is needed to understand these relationships and associated kinetic isotope effects.

This study highlights the importance of considering various physicochemical influences (other than temperature) on the degree of minor or trace cation isotopic fractionation in inorganic and biogenic minerals (e.g. $\delta^{88/86}Sr$ and $\delta^{26/24}Mg$ in $CaCO_3$) and the need to develop theoretical approaches/methods to calculate solution-solid fractionation factors which might be important when comparing fractionation factors between different minerals.

ACKNOWLEDGMENTS

A special thanks to A. Eisenhauer for the opportunity to run some samples at IFM-GEOMAR, J. Fitzpatrick for analytical help at the USGS-Menlo Park, and D. Lemarchand for earlier discussions about our initial results. R. Jones and G. Li provided valuable assistance with the SEM and ICP analyses. The authors thank the following core repositories for providing samples: Scripps Institute of Oceanography; Lamont Doherty Earth Observatory; Oregon State University; Florida State University; the Bremen Core Repository; and the University of Rhode Island Core Repository. We thank P. Lonsdale, M. Tivey, T. Naehr, and D. Stakes for generously sharing their barite samples with us. We thank M. Fantle and an anonymous reviewer for their very helpful comments and M. Rehkämper for his editorial handling. This work was funded by NSF CAREER Grant OCE-0449732 to A.P. and NSF EAR-0345433 to E.A.S. E.M.G. was supported by a National Defense Science and Engineering Graduate Fellowship while working on this project and is currently supported as a National Science Foundation Graduate Research Fellow.

REFERENCES

Amini M., Eisenhauer A., Böhm F., Fietzke J., Bach W., Garbe-Schönberg D., Rosner M., Bock B., Lackschewitz K. S. and Hauff F. (2008) Calcium isotope ($\delta^{44/40}Ca$) fractionation along hydrothermal pathways, Logatchev field (Mid-Atlantic Ridge, 14°45′N). *Geochim. Cosmochim. Acta* **72**, 4107–4122.

Averyt K. B. and Paytan A. (2003) Empirical partition coefficients for Sr and Ca in marine barite: implications for reconstructing seawater Sr and Ca concentrations. *Geochem. Geophys. Geosyst.* **4**(5), 1043. doi:10.1029/2002GC000426, ISSN: 1525-2027.

Bakó I., Hutter J. and Palinkas G. (2002) Car-Parrinello molecular dynamics simulation of the hydrated calcium ion. *J. Chem. Phys.* **117**, 9838–9843.

Bigeleisen J. and Mayer M. G. (1947) Calculation of equilibrium constants for isotopic exchange reactions. *J. Chem. Phys.* **15**, 261–267.

Bishop J. K. B. (1988) The barite-opal-organic carbon association in oceanic particulate matter. *Nature* **311**, 341–343.

Broecker W. S. and Peng T. -H. (1982) *Tracers in the Sea*. Lamont-Doherty Geologic Observatory.

Bruneval F., Donadio D. and Parrinello M. (2007) Molecular dynamics study of the solvation of calcium carbonate in water. *J. Phys. Chem. B* **111**, 12219–12227.

Bullen T. D., Krabbenhoft D. and Kendall C. (1996) Kinetic and mineralogic controls on the evolution of groundwater chemistry and $^{87}Sr/^{86}Sr$ in a sandy silicate aquifer, northern Wisconsin. *Geochim. Cosmochim. Acta* **60**, 1807–1821.

Chow T. J. and Goldberg E. D. (1960) On the marine geochemistry of barium. *Geochim. Cosmochim. Acta* **20**, 192–198.

Church T. M. (1970) Marine barite. Ph.D. thesis, University of California, San Diego.

Conkright M. E., Levitus S., O'Brien T., Boyer T. P., Antonov J. I. and Stephens C. (1998) World Ocean Atlas 1998 CD-ROM Data Set Documentation. In *Tech. Rep*. 15, pp. 16. NODC Internal Report.

Cowley E. R. and Pant A. K. (1973) Lattice dynamics of calcite. *Phys. Rev. B* **8**, 4795–4800.

Criss R. E. (1999) *Principles of stable isotope distribution*. Oxford University Press.

Dawson P., Hargreave M. M. and Wilkinson G. R. (1977) Polarized I. R. reflection, absorption, and laser Raman studies on a single crystal of $BaSO_4$. *Spectrochim. Acta* **35A**, 83–93.

De La Rocha C. L. and DePaolo D. J. (2000) Isotopic evidence for variations in the marine calcium cycle over the Cenozoic. *Science* **289**, 1176–1178.

Dehairs F., Chesselet R. and Jedwab J. (1980) Discrete suspended particles of barite and the barium cycle in the open ocean. *Earth Planet. Sci. Lett.* **49**, 528–550.

Eagle M., Paytan A., Arrigo K. R., Dijken G. v. and Murray R. W. (2003) A comparison between excess barium and barite as indicators of carbon export. *Paleoceanography* **18**(1), 1021:1-13.

Elderfield H. and Schultz A. (1996) Mid-ocean ridge hydrothermal fluxes and the chemical composition of the ocean. *Annu. Rev. Earth Planet. Sci.* **24**, 191–224.

Fantle M. S. and DePaolo D. J. (2005) Variations in the marine Ca cycle over the past 20 million years. *Earth Planet. Sci. Lett.* **237**, 102–117.

Fantle M. S. and DePaolo D. J. (2007) Ca isotopes in carbonate sediment and pore fluid from ODP Site 807A: the Ca^{2+}(aq)-calcite equilibrium fractionation factor and calcite recrystallization rates in Pleistocene sediments. *Geochim. Cosmochim. Acta* **71**, 2524–2546.

Farkaš J., Buhl D., Blenkinsop J. and Veizer J. (2007) Evolution of the oceanic calcium cycle during the late Mesozoic: evidence from $\delta^{44/40}Ca$ of marine skeletal carbonates. *Earth Planet. Sci. Lett.* **253**(1–2), 96–111.

Fulton J. L., Heald S. M., Badyal Y. S. and Simonson J. M. (2003) Understanding the effects of concentration on the solvation structure of Ca^{2+} in aqueous solution. I: the perspective on local structure from EXAFS and XANES. *J. Phys. Chem. A* **107**, 4688–4696.

Ganeshram R. S., Francois R., Commeau J. and Brown-Leger S. L. (2003) An experimental investigation of barite formation in seawater. *Geochim. Cosmochim. Acta* **67**, 2599–2605.

Graf D. L. (1961) Crystallographic tables for the rhombohedral carbonates. *Am. Mineral.* **46**, 1283–1316.

Griffith E. M., Paytan A., Kozdon R., Eisenhauer A. and Ravelo A. C. (2008) Influences on the fractionation of calcium isotopes in planktonic foraminifera. *Earth Planet. Sci. Lett.* **268**, 124–136.

Gussone N., Böhm F., Eisenhauer A., Dietzel M., Heuser A., Teichert B. M. A., Reitner J., Worheide G. and Dullo W.-C. (2005) Calcium isotope fractionation in calcite and aragonite. *Geochim. Cosmochim. Acta* **69**, 4485–4494.

Gustafsson, J. P. (2007) Visual MINTEQ Version 2.52. [Online] Available from: <http://www.lwr.kth.se/English/OurSoftware/vminteq/>.

Hawthorne F. C. and Ferguson R. B. (1975) Anhydrous sulphates, II. Refinement of the crystal structure of anhydrite. *Can. Mineral.* **13**, 289–292.

Hellwege K. H., Lesch W., Plihal M. and Schaack G. (1977) Zweiphononen-Absorptionsspektren end Dispersion der Schwingungszweige in Kristallen der Kalkspatstruktur (Translated title: "Two phonon absorption spectra and dispersion of phonon branches in crystals of calcite structure). *Zeitschrift fur Physik* **232**, 61–86.

Hennessy A. J. B. and Graham G. M. (2002) The effect of additives on the co-crystallisation of calcium with barium sulphate. *J. Cryst. Growth* **237–239**, 2153–2159.

Hensley T. M. 2006. Calcium isotopic variation in marine evaporites and carbonates: applications to Late Miocene Mediterranean brine chemistry and Late Cenozoic calcium cycling in the oceans. Ph.D., Univ. of California, San Deigo.

Heuser A., Eisenhauer A., Gussone N., Bock B., Hansen B. T. and Nägler T. F. (2002) Measurement of calcium isotopes ($\delta^{44}Ca$) using a multicollector TIMS technique. *Int. J. Mass Spectrom.* **220**, 385–397.

Heuser A., Eisenhauer A., Böhm F., Wallmann K., Gussone N., Pearson P. N., Nägler T. F. and Dullo W.-C. (2005) Calcium isotope ($\delta^{44/40}Ca$) variations of Neogene planktonic foraminifera. *Paleoceanography* **20**(PA2013), 1–13. doi:10.1029/2004PA001048.

Hippler D., Schmitt A-D., Gussone N., Heuser A., Stille P., Eisenhauer A. and Nägler T. F. (2003) Ca isotopic composition of various standards and seawater. *Geostandard Newslett.* **27**, 13–19.

Jacobsen S. D., Smyth J. R., Swope R. J. and Downs R. T. (1998) Rigid-body character of the SO_4 groups in celestine, anglesite and barite. *Can. Mineral.* **36**, 1053–1060.

Jones F., Oliviera A., Parkinson G. M., Rohl A. L., Stanley A. and Upson T. (2004) The effect of calcium ions on the precipitation of barium sulphate 1: calcium ions in the absence of organic additives. *J. Cryst. Growth* **262**, 572–580.

Kasemann S. A., Hawkesworth C. J., Prave A. R., Fallick A. E. and Pearson P. N. (2005) Boron and calcium isotope composition in Neoproterozoic carbonate rocks from Namibia: evidence for extreme environmental change. *Earth Planet. Sci. Lett.* **231**, 73–86.

Kowacz M., Putnis C. V. and Putnis A. (2007) The effect of cation:anion ratio in solution on the mechanism of barite growth at constant supersaturation: role of desolvation on the growth kinetics. *Geochim. Cosmochim. Acta* **71**, 5168–5179.

Legg M. R. 1980 Seismicity and tectonics of the inner continental borderland of southern California and northern Baja California, Mexico. M.S. thesis, Univ. of California, San Diego.

Lemarchand D., Wasserburg G. J. and Papanstassiou D. A. (2004) Rate-controlled calcium isotope fractionation in synthetic calcite. *Geochim. Cosmochim. Acta* **68**, 4665–4678.

Lonsdale P. (1979) A deep-sea hydrothermal site on a strike-slip fault. *Nature* **281**, 531–534.

Lonsdale P. and Becker K. (1985) Hydrothermal plumes, hot springs, and conductive heat flow in the Southern Trough of Guaymas Basin. *Earth Planet. Sci. Lett.* **73**(2–4), 211–225.

Martin E. E., Macdougall J. D., Herbert T. D., Paytan A. and Kastner M. (1995) Strontium and neodymium isotopic analyses of marine barite separates. *Geochim. Cosmochim. Acta* **59**, 1353–1361.

Méheut M., Lazzeri M., Balan E. and Mauri F. (2007) Equilibrium isotopic fractionation in the kaolinite, quartz, water system: prediction from first-principles density-functional theory. *Geochim. Cosmochim. Acta* **71**, 3170–3181.

Monkhorst H. J. and Pack J. D. (1976) Special points for Brillouin-zone integrations. *Phys. Rev. B* **13**, 5188–5192.

Monnin C. and Cividini D. (2006) The saturation state of the world's ocean with respect to (Ba, Sr)SO_4 solid solutions. *Geochim. Cosmochim. Acta* **70**, 3290–3298.

Monnin C., Jeandel C., Cattaldo T. and Dehairs F. (1999) The marine barite saturation state of the world's oceans. *Mar. Chem.* **65**, 253–261.

Paytan A. (1996) Marine barite: a recorder of oceanic chemistry, productivity and circulation. Ph.D. thesis, Univ. of California, San Diego.

Paytan A., Kastner M., Martin E. E., Macdougall J. D. and Herbert T. (1993) Marine barite as a monitor of seawater strontium isotope composition. *Nature* **366**, 445–449.

Paytan A., Mearon S., Cobb K. and Kastner M. (2002) Origin of marine barite deposits: Sr and S isotope characterization. *Geology* **30**(8), 747–750.

Perdew J. P., Burke K. and Ernzerhof M. (1996) Generalized gradient approximation made simple. *Phys. Rev. Lett.* **77**, 3865–3868.

Pilson M. E. Q. (1998) *An Introduction to the Chemistry of the Sea*. Prentice-Hall Inc.

Porto S. P. S. (1966) Depolarization of Raman scattering in calcite. *Phys. Rev.* **147**, 608–611.

Reyes A. O., Moore W. S. and Stakes D. S. (1995) Th-228/R-228 ages of a Barite-rich chimney from the endeavor segment of the Juan-De-Fuca ridge. *Earth Planet. Sci. Lett.* **131**(1–2), 99–113.

Rutt H. N. and Nicola J. H. (1974) Raman spectra of carbonates of calcite structure. *J. Phys. C Solid State* **7**, 4522–4528.

Schauble E. A. (2004) Applying stable isotope fractionation theory to new systems. In *Geochemistry of non-traditional stable isotopes* vol. 55 (eds. C. M. Johnson, B. Beard, and F. Albarede), pp. 65–111.

Schauble E. A., Ghosh P. and Eiler J. M. (2006) Preferential formation of ^{13}C–^{18}O bonds in carbonate minerals, estimated using first-principles lattice dynamics. *Geochim. Cosmochim. Acta* **70**, 2510–2529.

Schmitt A. D., Chabaux F. and Stille P. (2003a) The calcium riverine and hydrothermal isotopic fluxes and the oceanic calcium mass balance. *Earth Planet. Sci. Lett.* **213**(3–4), 503–518.

Schmitt A. D., Stille P. and Vennemann T. (2003b) Variations of the $^{44}Ca/^{40}Ca$ ratio in seawater during the past 24 million years: evidence from $\delta^{44}Ca$ and $\delta^{18}O$ values of Miocene phosphates. *Geochim. Cosmochim. Acta* **67**, 2607–2614.

Shannon R. D. (1976) Revised effective ionic radii and systematic studies of interatomic distances in halides and chalcogenides. *Acta Crystallogr.* **A32**, 751–767.

Sime N. G., De La Rocha C. L., Tipper E. T., Tripati A., Galy A. and Bickle M. J. (2007) Interpreting the Ca isotope record of marine biogenic carbonates. *Geochim. Cosmochim. Acta* **71**, 3979–3989.

Skulan J., DePaolo D. J. and Owens T. L. (1997) Biological control of calcium isotopic abundances in the global calcium cycle. *Geochim. Cosmochim. Acta* **61**, 2505–2510.

Skulan J., Bullen T. D., Anbar A. D., Puzas J. E., Schackelford L., LeBlanc A. and Smith S. M. (2007) Natural calcium isotopic composition of urine as a marker of bone mineral balance. *Clin. Chem.* **53**(6), 1155–1158.

Soudry D., Segal I., Nathan Y., Glenn C. R., Halicz L., Lewy Z. and VonderHaar D. L. (2004) $^{44}Ca/^{42}Ca$ and $^{143}Nd/^{144}Nd$ isotope variations in cretaceous-eocene Tethyan francolites and their bearing on phosphogenesis in the southern Tethys. *Geology* **32**(5), 389–392.

Steuber T. and Buhl D. (2006) Calcium-isotope fractionation in selected modern and ancient marine carbonates. *Geochim. Cosmochim. Acta* **70**, 5507–5521.

Stroobants N., Dehairs F., Goeyens L., Vanderheijden N. and Grieken R. V. (1991) Barite formation in the Southern Ocean water column. *Mar. Chem.* **35**, 411–421.

Tang J., Dietzel M., Bohm F., Kohler S. J. and Eisenhauer A. (2008) Sr^{2+}/Ca^{2+} and $^{44}Ca/^{40}Ca$ fractionation during inorganic calcite formation: II. Ca isotopes. *Geochim. Cosmochim. Acta* **72**, 3733–3745.

Teichert B. M. A., Gussone N., Eisenhauer A. and Bohrmann G. (2005) Clathrites: archives of near-seafloor pore-fluid evolution ($\delta^{44/40}Ca$, $\delta^{13}C$, $\delta^{18}O$) in gas hydrate environments. *Geology* **33**(3), 213–316.

Tivey M. K., Humphries S. E., Thompson G., Hannington M. D. and Rona P. A. (1995) Deducing patterns of fluid flow and mixing within the TAG active hydrothermal mound using mineralogical and geochemical data. *J. Geophys. Res.* **100**, 12527–12555.

Torres M. E., McManus J. and Huh C. A. (2002) Fluid seepage along the San Clemente Fault scarp: basin-wide impact on barium cycling. *Earth Planet. Sci. Lett.* **203**, 181–194.

Urey H. C. (1947) The thermodynamic properties of isotopic substances. *J. Chem. Soc. (London)*, 562–581.

Wahid F. A., Thomson G. B., Graham G. M. and Jackson R. A. (2002) A computational study of the effect of doping covalent cations in barite. *J. Mater. Chem.* **12**, 3799–3802.

Wu Z. and Cohen R. E. (2006) More accurate generalized gradient approximation for solids. *Phys. Rev. B* **73**, 235116.

Zhu P. and Macdougall J. D. (1998) Calcium isotopes in the marine environment and the oceanic calcium cycle. *Geochim. Cosmochim. Acta* **62**, 1691–1698.

Associate editor: Mark Rehkamper